MATERIAL AND METHODS

Dye characterization for ratiometric real-time imaging of NO in vitro

We first assessed suitability of DAA, as a NO-sensitive fluorophore and Alexa 633, as a reference dye indicator, for ratiometric NO imaging. Using a 488 nm excitation wavelength, we tested whether emission spectra of dyes overlapped. Lambda scan analysis was performed to measure the intensity of fluorescence relative to different emission wavelengths. DAA under these conditions had maximal emission between 500 to 525 nm, whereas Alexa 633 had maximal emission from 600 to 620 nm (Fig S2A). Thus the two well defined emission peaks were easily separated when a mixture of the two dyes was ejected to the tissue.

DAA sensitivity to NO was tested by adding to the bath a NO-donor at two different concentrations (Fig S2B-D). When dyes were ejected into agar (2.5% in aCSF), fluorescence intensity dropped slightly slower for DAA than for Alexa 633 over time, as indicated by the negative slope (Slope (S) = $-0.8 \pm 0.9 \times 10^{-2}$ a.u./s; n = 12) of the ratio DAA/Alexa 633 (Fig S2D). The DAA/Alexa 633 ratio, however, increased linearly in a dose-dependent way when the NO-donor DEA/NO was added to the bath ($S=0.6 \pm 0.3 \times 10^{-2}$ a.u./s and $S=1.9 \pm 0.9 \times 10^{-2}$ a.u./s for 1 and 10 μM of DEA/NO, respectively; n = 4 experiments per concentration; Fig S2D). The slope of the DAA/Alexa 633 ratio was much higher when dyes were ejected into brainstem slices ($S = 2.8 \pm 0.4 \times 10^{-2}$ a.u./s and $S = 6.2 \pm 1.2 \times 10^{-2}$ a.u./s for 1 and 10 μM of DEA/NO; n= 20 and 16, respectively; Fig S2B-D). These results indicate that DAA is a suitable NO-sensitive dye in our experimental conditions and that the slope of the DAA/Alexa 633 ratio is a useful index to detect NO synthesis.

Immunohistochemistry

Immunohistochemical detection of the astroglial cells marker glial fibrillary acidic protein (GFAP) was performed in sections obtained from animals which received unilateral intranuclear administration of viral vectors to control against possible contamination of the results by astroglial transfection. Free-floating sections were rinsed in PBS and immersed in 2.5% (w/v) bovine serum albumin, 0.25% (w/v) sodium azide, and 0.1% (v/v) Triton X-100 in PBS for 30 min, followed by overnight incubation at 4°C with a rabbit polyclonal anti-GFAP antibody (1:5,000; Dako). Subsequently, the tissue was rinsed in PBS and incubated for 2 h at room temperature with an anti-rabbit IgG labeled with cyanine 5 (Cy5) (1:200; Jackson ImmunoResearch, West Grove, PA) and then washed with PBS. Omission of primary antibody resulted in no detectable staining. Slides were analyzed using an Olympus (Tokyo, Japan) BX60 epifluorescence microscope or a Leica Spectral confocal microscope.

Western blotting

Area of brainstem containing HN was dissected from sacrificed animals injected with different constructs. It is important to note that we could not exclusively extract only the transduced neurons of HN, and the tissues in all cases contained some of the adjacent brainstem structures. For that reason degree of nNOS knock-down in the actual HMNs is an underestimate because the samples always contained some un-transduced cells. Total protein was extracted from homogenized samples, followed by quantification with BCA protein assay kit (Pierce). 20 μg of total protein per lane were separated on NuPAGE 4-12% Bis-Tris gels (Invitrogen) and transferred to PVDF membranes (Millipore). The membranes were blocked in 5% non-fat dry milk (NFDM)

in TBS (Tris-buffered saline) with 0.1% tween-20 (TBST) for 45 min, and incubated with polyclonal rabbit anti-nNOS antibody (Zymed) at 1:5000 in 3% NFDM-TBST or monoclonal anti-β-actin antibody (Sigma) at 1:5000 in 1% BSA-TBST overnight. Following incubation with polyclonal swine anti-rabbit immunoglobulins/HRP (Dako) at 1:5000 in 3% NFDM-TBST or polyclonal rabbit anti-mouse immunoglobulins/HRP (Dako) at 1:10000 in 1% BSA-TBST for 90 min, the immunoreactivities were detected with Immun-Star Western chemiluminescent kit (Bio-Rad) and Amersham high performance autoradiography film (GE Healthcare). Scion Image software was used to quantitatively compare the relative blot intensities.

RESULTS

Characterization of retrograde transfection of HMNs after AVV injection into the tongue

Peripheral administration of adenoviral vectors may result in transduction of central efferent structures via retrograde route. Given that the main objective of this work was to study the role of nNOS over-expression on alterations in the electrophysiological properties of motoneurons induced by motor nerve injury, we first investigated transfection and distribution pattern of gene expression after peripheral injection of AVV. We injected up to 300 µl of a mixture of AVV-eGFP/AVV-mRFP (1:1) into the tip of the tongue of adult rats. One week after injection, some scattered motoneurons (36.5 ± 7.6 transfected-HMNs/rat, ranging from 8 to 70; n = 8 animals) were transfected, though a high degree of co-transfection was observed (>90% of eGFP-positive HMNs also expressed mRFP; Fig S3A). The pattern of expression did not change during the next week, judging by a similar number and distribution of transfected HMNs at 15 days after adenoviral administration (data not shown). Based on these results we decided against retrograde transduction for electrophysiological experiments, due to the low probability of recording a transduced motoneuron. However, we can assume a high probability of studying a nNOS-transfected motoneuron when animals were infected with AVV-eGFP/AVV-nNOS directly into HN.

Characterization of intranuclear microinjection of AVV

For functional studies we injected AVV directly into the HN (Fig S3B). This study included only recordings obtained from rats in which the injection was verified post-mortem to be restricted within the limits of the HN. Five to seven days after

adenoviral administration, numerous neurons were identified as positively transfected at the injection site. Besides, a high number of astrocytes were also transfected, as confirmed by co-immunostaining against the astroglial cell marker GFAP (Fig S3C, D). Inspection of brainstem slices did not reveal eGFP-positive cell bodies in projection areas to the HN, such as the ventrolateral reticular formation (VLRF in Fig S3E). This argues against the possibility that our results could be affected by retrograde spread of the AVV from the site of injection. A large number of eGFP-positive neurons were identified strictly within the HN, 200-300 μm rostrocaudal and ipsilateral to the injection site (Fig S3F). Most of them also co-expressed mRFP when AVV-eGFP and AVV-mRFP were co-injected (Fig S3G, H). Furthermore, astroglia was not transduced at these remote locations, as co-localization of eGFP and GFAP was absent there (Fig S3I). Therefore, functional tests were performed in these areas away from the injection site to minimize any contaminating effects of nNOS expression in astrocytes.

Characterization of intranuclear LVV injection

Given that adenoviruses with CMV promoter can also express genes in glial and endothelial cells and retrogradely infect afferent neurons to the HN, results could be partially distorted by these unspecific properties of the vectors. Moreover, intracerebral microinjection could cause a surgical trauma, which can up-regulate nNOS and initiate the expression of inducible NOS (iNOS) in the proximity of the lesion (Rao et al., 1999; Petrov et al., 2000), therefore creating a non-physiological source of NO production. To isolate specific effects due to neuronal expression in the HN, a mixture of two lentiviral vectors was used. Lentiviral vectors used in this study were pseudotyped with VSVG coat protein which is widely known to prevent retrograde transduction. Lentiviruses (abbreviated as LVV-miR-shRNA/nNOS) direct the expression of eGFP upstream a

shRNA targeting mRNA for nNOS specifically in neurons by a Tet-off transactivation system regulated by the synapsin-1 promoter (Liu et al., 2008). One week after lentivirus injection into the HN, a high number of transduced neurons was observed (Fig S3J, K). At the same time GFAP-identified astrocytes essentially never expressed the transgene even directly within the injection site (Fig S3J). Expression of the LVV-miR-shRNA/nNOS was drastically reduced by supplementing the drinking water with Dox, which binds to the Tet-off transactivator, blocks activation of the TET promoter and shuts down the eGFP-miR-shRNA transcription (Fig S3L). In addition, intranuclear co-injection of AVV-mRFP and LVV-miR-shRNA/nNOS resulted in high frequency of co-transduction (Fig S3K). For these reasons, and given the rostrocaudal size of the injection extension (total extent: 418.8 ± 18.2 μm; n = 32 injections), to avoid the contaminating influence of undesired NO sources the study included only recordings performed at least at a distance of 200 μm from the injection site.

Recruitment scheme of the HMN pool after AVV-nNOS-transduction

Cumulative sum histograms were well fitted by the exponential function and demonstrated that the proportion of motor units that would have been active at 0% of ET_{CO2} in the AVV-eGFP/AVV-nNOS group (~63 %) was much higher than in the AVV-eGFP-treated pool (~21 %) (Fig S4). The alteration in the percentage of motor units recruited was similar to that induced by nerve injury (intact: ~36 %; 7 days after crushing: ~62 %; Fig S4). These disturbances were indeed accompanied by a reduction in the recruitment gain (i.e., the recruitment rate throughout the whole ET_{CO2} range) (Fig S4B, compare exponential growth rates). As in the control condition, chronic inhibition of either sGC activity with ODQ or nNOS disruption by preceding LVV-miR-shRNA/nNOS injection in both the AVV-nNOS-treated or crushed groups

preserved the recruitment arrangement of motor units, although they were slightly shifted toward higher Ths. LVV-miR-shRNA/nNOS effect was absent in Dox-treated rats (Fig S4B).

SUPPLEMENTARY FIGURES

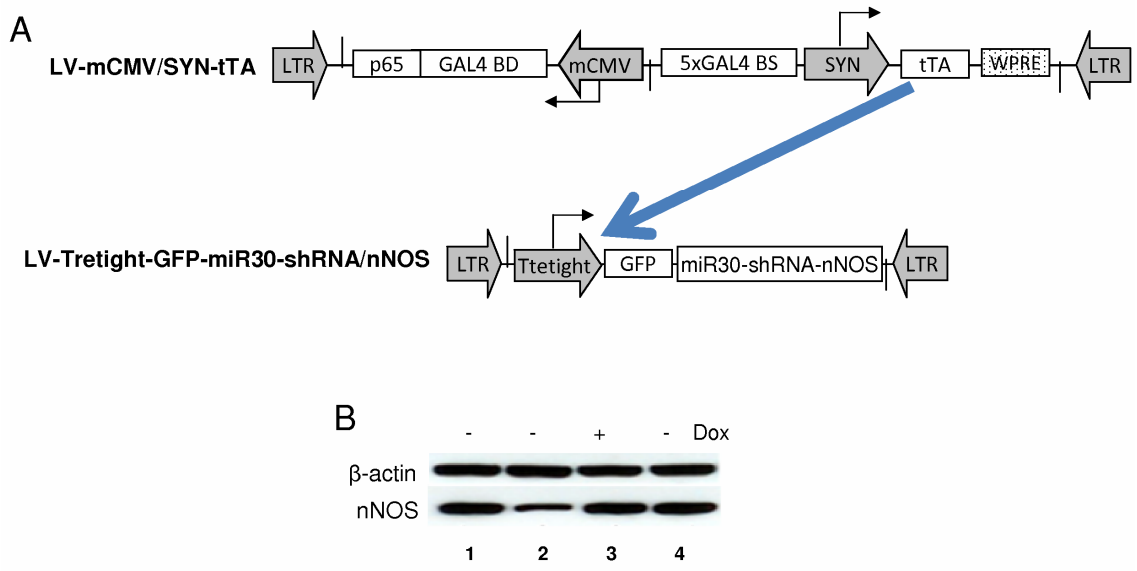

Figure S1.- LVV-miR-shRNA/nNOS down-regulates nNOS in the HN. ***A*****,** Schematic layout of the binary lentiviral system to express miR-shRNA in neurons selectively under control of amplified synapsin-1 promoter (SYN). The system is based on design originally published by Stegmeier et al., 2005 and Liu et al 2008. ***B*****,** Western blot analysis of nNOS knock down *in vivo.* Efficacy of nNOS knock-down was tested in separate experiments in groups of 3 rats. Group 1 was control and not injected. Groups 2 and 3 received anti-nNOS miR-shRNA into the hypoglossal nucleus area of brainstem. 1-2 weeks later tissue was processed for Western blotting using standard procedures. In group 4 a LVV system targeting luciferase was injected as a negative control. Note strong reduction in nNOS protein in the second group and lack of nNOS knock-down in animals kept on Dox (group 3, see main text for details). Densitometric analysis of the bands revealed ~50% nNOS knock down in group 2. β-actin was used as a reference to ensure equal protein loading.

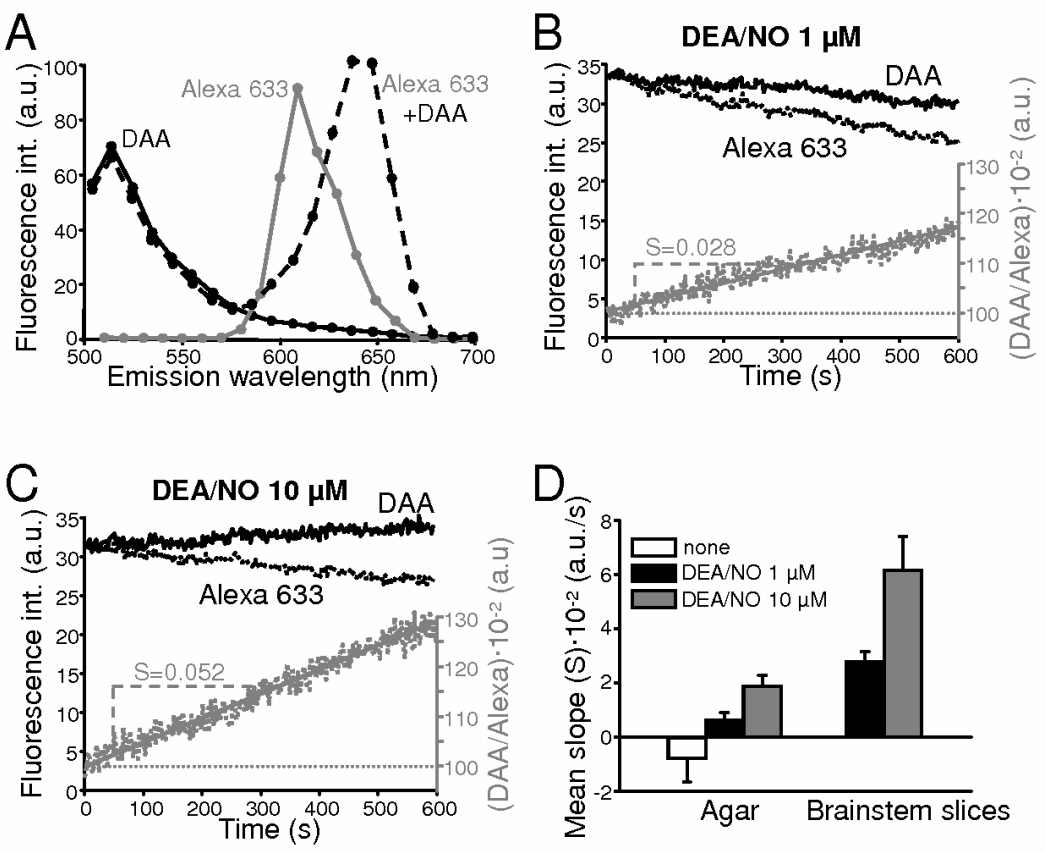

Figure S2.- Real-time imaging of NO. ***A*****,** Lambda scan analysis illustrating DAA and Alexa 633 spectra emission. Plot showing the fluorescence intensity (int.), in arbitrary units (a.u.), of the indicated fluorophores ejected alone or together through the micropipettes using a 488 nm excitation wavelength. Note that when both dyes were ejected together the maximal intensity of fluorescence for Alexa 633 was displaced to higher wavelengths. ***B*****,** ***C*****,** Time course of the fluorescence intensity (left y-axis) of two dyes ejected in brainstem slices after addition to the perfusate of 1 (B) or 10 (C) µM DEA/NO. The slope (S; a.u./s) of the regression lines of the ratio between the fluorescence intensity of DAA and Alexa 633 channels ((DAA/Alexa 633)·100) was taken as an index of NO concentration. ***D*****,** Mean slope of the DAA/Alexa ratio under the indicated conditions when recordings and dye ejection were performed into agar (2.5% in aCSF; None, n = 12; DEA/NO 1 µM, n = 4; DEA/NO 10 µM, n = 4) or into brainstem slices (DEA/NO 1 µM, n = 20; DEA/NO 10 µM, n = 16).

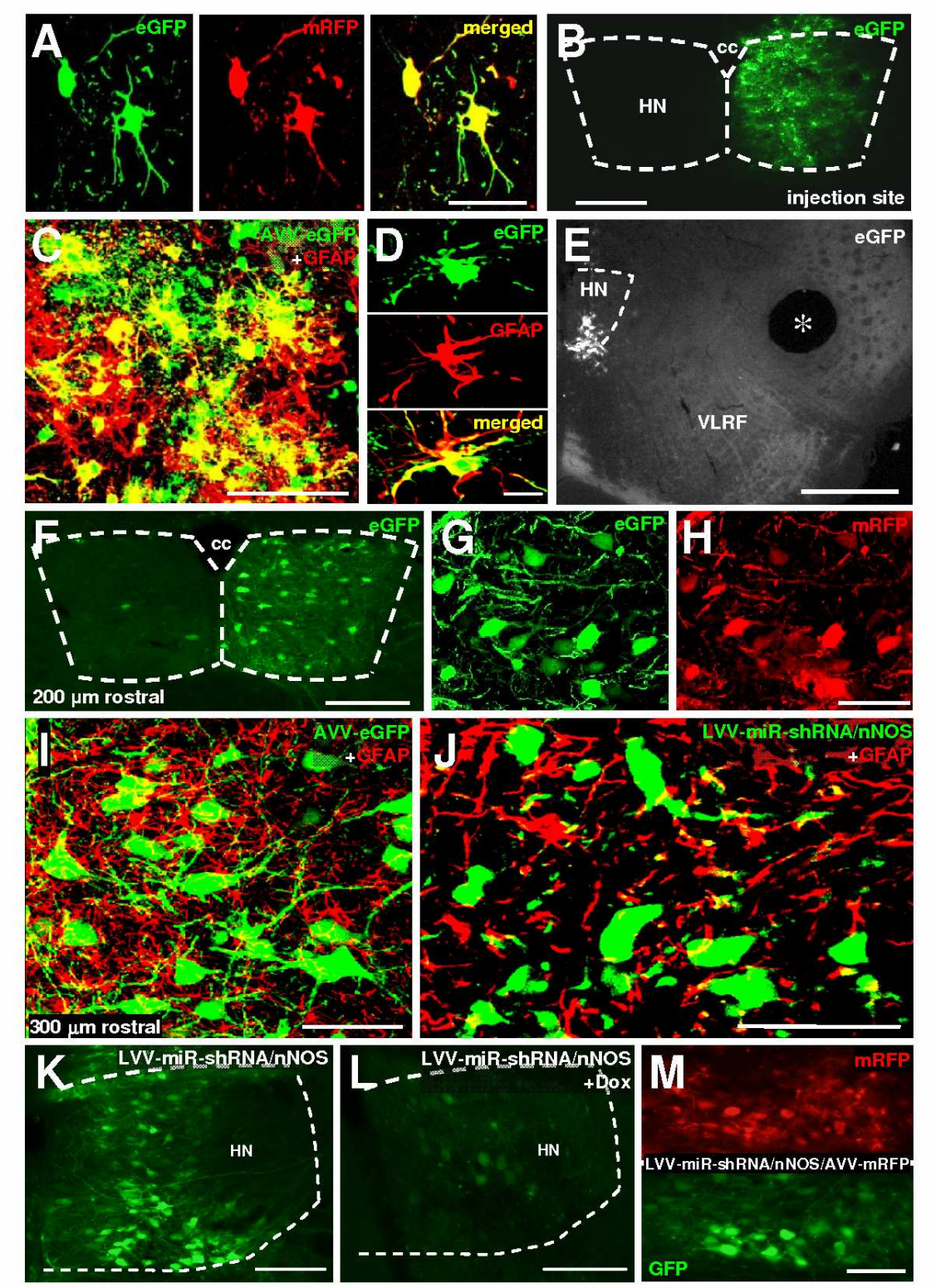

Figure S3.- Specificity of viral injections and transfections. A, Confocal photomicrographs showing two HMNs co-expressing eGFP and mRFP obtained 7 days after AVV-eGFP/AVV-mRFP injection into the tip of the tongue. ***B*****,** Epifluorescence photomicrograph of a coronal section at the level of the hypoglossal nucleus (HN)

obtained 6 days after intranuclear injection of AVV-eGFP. Note that injection was almost fully restricted to the HN. ***C*, *D*,** Immunohistochemistry against GFAP showed a high proportion of astrocytes expressing eGFP at the injection site of AVV-eGFP into the HN (C). A high magnification photomicrograph showing an infected astrocyte is presented in D. ***E*,** Low magnification photomicrograph of a coronal section at the level of AVV-eGFP injection site, obtained 7 days after viral administration. Note the absence of infected neurons in neighboring regions, such as the ventrolateral reticular formation (VLRF), which project directly to the HN. Asterisk points to the mark performed to identify the right side of the brainstem. ***F-H*,** Photomicrograph of a coronal section obtained 7 days after viral administration at the indicated distance from the injection site showing a broad number of eGFP-expressing hypoglossal neurons (F). At this level a high frequency of co-transfection was observed after intranuclear injection of AVV-eGFP/AVV-mRFP (G,H); cc, central canal. ***I*,** Confocal photomicrograph of a coronal section immunolabeled for GFAP at the indicated level from the AVV-eGFP injection site illustrating the absence of infected astroglia. ***J*,** Immunohistochemistry against GFAP at the level of the LVV-miR-shRNA/nNOS injection site illustrating the absence of transfected astrocytes. ***K*, *L*,** Photomicrographs from coronal sections at the level of the injection place obtained 7 days after intranuclear injection of LVV-miR-shRNA/nNOS in untreated animals (K) or receiving doxycycline (Dox) in the drinking water (L). ***M*,** A high frequency of co-transduction was also obtained after co-injection into the HN of AVV-mRFP and LVV-miR-shRNA/nNOS. Calibration bars: 15 μm in D, 100 μm in A, C, H-M, 250 μm in B, F and 500 μm in E.

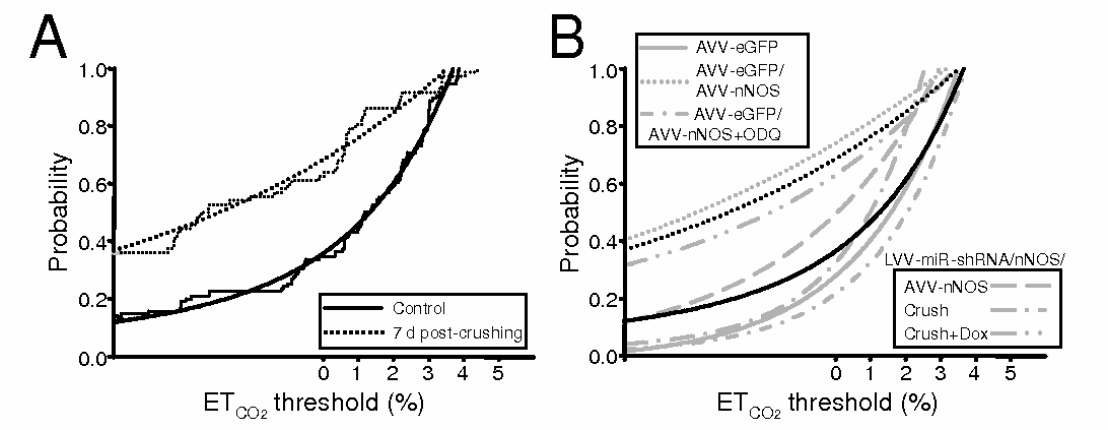

Figure S4.- AVV-nNOS injection into the HN mimics changes in the recruitment scheme of HMNs induced by XIIth nerve crushing. ***A*****,** Cumulative probability histograms of Th obtained in control and at 7 days post-lesion. Histograms were fitted by exponential growing functions ($r > 0.95$, $P < 0.0001$). ***B*****,** For clarity in the comparison only exponential curves fitted to each motoneuron pool at the indicated conditions are plotted. Exponential functions are as follows: control: $y = 0.07 + 0.37 \cdot \exp(0.2 \cdot x)$; 7 d post-crushing: $y = 0.03 + 0.6 \cdot \exp(0.11 \cdot x)$; AVV-eGFP: $y = -0.02 + 0.3 \cdot \exp(0.35 \cdot x)$; AVV-eGFP/AVV-nNOS: $y = -0.12 + 0.86 \cdot \exp(0.08 \cdot x)$; AVV-eGFP/AVV-nNOS+ODQ: $y = 0.01 + 0.21 \cdot \exp(0.42 \cdot x)$; LVV-miR-shRNA/nNOS/AVV-nNOS: $y = 0.01 + 0.21 \cdot \exp(0.42 \cdot x)$; LVV-miR-shRNA/nNOS/crush: $y = 0.02 + 0.30 \cdot \exp(0.46 \cdot x)$; LVV-miR-shRNA/nNOS/crush+Dox: $y = 0.12 + 0.51 \cdot \exp(0.16 \cdot x)$. The number of analyzed HMNs per condition is indicated in Table 2.